OPEN ACCESS
IOP Publishing
Journal of Physics D: Applied Physics
J. Phys. D: Appl. Phys. **56** (2023) 435204 (18pp)
https://doi.org/10.1088/1361-6463/ace97e

Static breakdown threshold modeling of quasi-uniform gas gaps with a focus on the PDIV of contacting enameled wire pairs

R Färber[1,*], Y Lu[1], M Balmelli[2], O Sefl[1] and C M Franck[1]

[1] High Voltage Laboratory, Department of Information Technology and Electrical Engineering, ETH Zurich, Physikstrasse 3, 8092 Zurich, Switzerland
[2] Empa, Swiss Federal Laboratories for Materials Science and Technology, Überlandstrasse 129, 8600 Dübendorf, Switzerland

E-mail: faerberr@ethz.ch

Received 25 May 2023
Accepted for publication 21 July 2023
Published 2 August 2023

Abstract

This paper provides a theoretical and conceptual framework for the determination of static breakdown inception thresholds in quasi-uniform gas gaps bounded by dielectric layers of thickness s and relative permittivity ε_r'. The special case of uncoated metallic electrodes is included in the limit $s/\varepsilon_r' \to 0$. Moreover, a review of breakdown mechanisms and the underlying physical processes in quasi-uniform gas gaps is provided, and the applicability of the associated breakdown criteria is discussed. The results include a parametrization of the partial discharge inception voltage of wedge-shaped air gaps at atmospheric pressure as a function of the reduced coating thickness s/ε_r'. The predicted results for this prototypical insulation geometry agree well with a broad array of literature data and own measurements. Finally, a physically motivated parametrization of the ionization threshold $K(d)$ is suggested for atmospheric pressure air in terms of secondary electron feedback by energetic photons and ion-enhanced field emission. This contrasts with the ad hoc introduction of modified 'streamer constants' often found in literature to explain breakdown voltages that deviate from the predictions of the classical Raether–Meek–Loeb criterion.

Keywords: partial discharge inception, gas discharge physics, electrical breakdown, streamer discharge, Townsend discharge, twisted pair, dielectric barrier discharge

(Some figures may appear in colour only in the online journal)

* Author to whom any correspondence should be addressed.

Symbol	Value	Unit	Name
α		m^{-1}	Ionization coefficient
α_{eff}		m^{-1}	Effective ionization coefficient
d		m	Gap length
E		$\mathrm{V}\cdot\mathrm{m}^{-1}$	Electric field
E_{g}		$\mathrm{V}\cdot\mathrm{m}^{-1}$	Electrode electric field value in the gas
E_{crit}		$\mathrm{V}\cdot\mathrm{m}^{-1}$	Critical electric field (above which $\alpha_{\mathrm{eff}} > 0$)
E_{b}		$\mathrm{V}\cdot\mathrm{m}^{-1}$	Static breakdown electric field
E_{th}		$\mathrm{V}\cdot\mathrm{m}^{-1}$	Threshold electric field value below which ionic space charge enhances the ionization yield of secondary avalanches
E/N		Td	Reduced electric field
e	$1.602\cdot10^{-19}$	C	Elementary charge
γ		—	Effective secondary electron emission coefficient
γ_{i}		—	Secondary electron emission coefficient due to positive ions
γ_{ph}		—	Secondary electron emission coefficient due to photoelectric effect at the cathode
ε_0	$8.854\cdot10^{-12}$	$\mathrm{F}\cdot\mathrm{m}^{-1}$	Permittivity of free space
$\underline{\varepsilon}_{\mathrm{r}}$	$\varepsilon_{\mathrm{r}}' - j\varepsilon_{\mathrm{r}}''$	—	Relative permittivity of the coating
η		m^{-1}	Electron attachment coefficient
j_0		$\mathrm{A}\cdot\mathrm{m}^{-2}$	Seed electron current density at the cathode surface
K		—	Ionization threshold
N		m^{-3}	Neutral gas density
n_{crit}		—	Critical number of electrons for single-avalanche streamer inception
p	$N\cdot k_{\mathrm{B}}\cdot T$	bar	Gas pressure (note: $T = 300$ K is used for the conversion between p and N)
U_{el}		V	Electrode voltage
U_{g}		V	Gap voltage
U_{b}	$\min(U_{\mathrm{T}}, U_{\mathrm{S}})$	V	Static breakdown voltage
U_{T}		V	Townsend threshold voltage
U_{S}		V	Single-avalanche streamer threshold voltage

1. Introduction

Since the discovery of static electricity, the electrical spark had been a well-known physical phenomenon. In the early 1700s, the English scientist Francis Hauksbee beautifully described the electric sparks he observed in the dark emanating from a glass tube rubbed by hand [1] (p 60):

> 'if another Hand was held near the Tube, a Light would evidently break forth from it, and That accompanied with a Noise, resembling that of the cracking of a green Leaf in the Fire'

It was not until much later, however, that the physical mechanisms underlying the formation of the electric spark were elucidated, starting at the turn of the 19th century with the first atomistic theory of breakdown developed at the Cavendish laboratory by a team of physicists—including J.S. Townsend—under the lead of J.J. Thomson [2].

Despite its long history, the theory of the electric breakdown of a gas—the abrupt transition of the insulating state into an electrically conducting plasma when a certain voltage threshold between the electrodes is exceeded—remained a subject of intense study throughout the 20th century up to the present time. Besides scientific curiosity, the sustained interest in the phenomenon is certainly also driven by its high practical relevance in numerous areas of technology, ranging from the design of particle detectors [3] to the dimensioning of new nanosecond pulsed ignition systems for internal combustion engines [4], to the determination of appropriate clearance distances in high voltage apparatus [5].

More recently, the determination of partial breakdown thresholds in so-called wedge-shaped gas gaps bounded by insulating dielectric coatings has attracted increasing attention due to its relevance in suppressing the ignition of unwanted dielectric barrier plasma discharges in the turn-to-turn insulation of electric motors driven by inverter output voltages [6–8]. The wedge-shaped gas gap bounded by a dielectric electrode coating, shown in figure 1(a), can be used to represent this type of insulation system. In such a gas gap, a partial electrical breakdown—by convention called a partial discharge (PD)—can occur when the electrode voltage exceeds a threshold known as the PD inception voltage (PDIV). The reason for the partial as opposed to complete breakdown of the configuration lies in the gas' lower electric strength compared to the solid insulation, as well as the electric field enhancement in the gas by the induced bound charges at the dielectric boundaries. If the insulation material is organic (e.g. a polymer), repetitive PDs cause its gradual erosion until a full breakdown terminates the lifetime of the insulation barrier [8]. Being able to determine the PDIV of wedge-shaped insulation geometries based on the relevant physical parameters of the system is thus

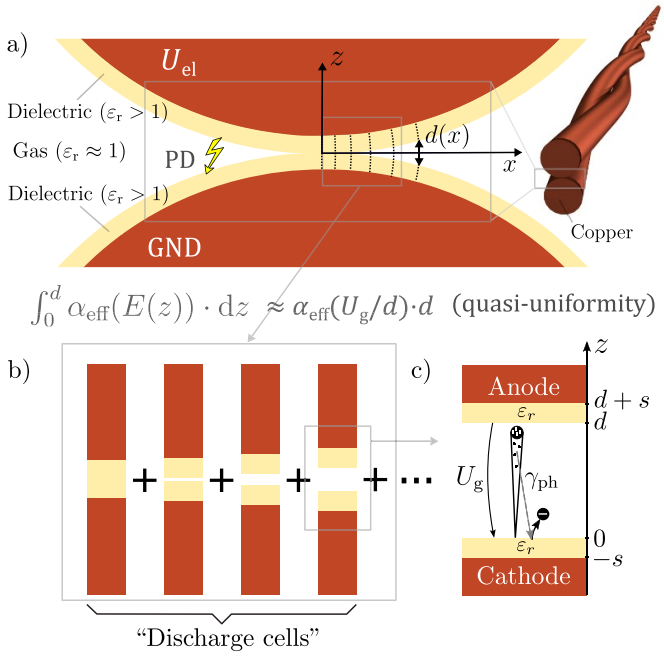

Figure 1. (a) A wedge-shaped gas gap bounded by dielectric electrode coatings representing, for instance, the turn-to-turn insulation in an electric motor winding. Typical wire diameters are on the order of 1 mm, while coating thicknesses range from roughly 20 μm to 100 μm. The coating is typically a polymeric material with a dielectric permittivity ε_r' between 2.5 and 5 (at room temperature). (b) Approximate reduction of the geometry in (a) to a parallel connection of uniform discharge cells. (c) Single discharge cell with an electron avalanche and the release of a secondary photo-electron at the cathode boundary. The special case of metallic electrodes is obtained by letting $s/\varepsilon_r' \to 0$.

of utmost importance for the reliable design of these insulation systems.

The quasi-universal approach for determining the (partial) breakdown voltage in gases—bounded by dielectric layers or not—is the application of a Townsend–Schumann–Loeb–Meek–Raether type criterion of the form [9–12]

$$\int \alpha_{\text{eff}} \cdot \mathrm{d}l \stackrel{!}{=} K, \tag{1}$$

where α_{eff} is the effective ionization coefficient, and the integral is performed along field lines in the region where $\alpha_{\text{eff}} > 0$, i.e. where the electric field is above the critical electric field E_{crit}. Breakdown can occur if the criterion is fulfilled along at least one field line (a suitably placed seed electron is also required to initiate the breakdown process). Unfortunately, the value of the so-called 'streamer constant' K predicting the measured breakdown voltages in various insulation configurations has been found to be less constant than its name suggests [13, 14], the main influencing variables being the the pressure p × gap distance d product and the gas type itself. For example, Malik [13] found K to vary from 1.4 to 74 for predicting breakdown voltages in a quasi-uniform electric field in air when $p \cdot d$ was varied from 0.01 bar · cm to 40 bar · cm. While the values of K above 23 are unphysical [15] ($e^{23} \approx 10^{10}$ avalanche electrons, $e^{74} \approx 10^{32}$) and caused by the sensitivity of the calculated K value on the zero-crossing of α_{eff} (see appendix C), the measurements do illustrate that the ionization threshold predicting the measured breakdown voltage can be significantly lower than the 'conventional' value $K = \ln(n_{\text{crit}}) \approx 18..20$ derived from the classical streamer theory [12]. The classical streamer theory imposes the condition that the electric field created by the space charge of the avalanche 'significantly' distorts the electrode field, which leads to $n_{\text{crit}} \approx 10^6..10^8$ for atmospheric pressure air [12, 16]. It will be shown in this paper that while the exact value of the parameter K is less relevant for the determination of breakdown voltages in large (mm to cm-sized) gaps (because variations in K produce only moderate changes in the calculated breakdown voltage), it *does* matter for small gap lengths ($d \ll 1$ mm), applying for example to the configuration shown in figure 1. Indeed, using the value $K = 18$ leads to an overestimation of the PDIV in these configurations by a factor of about 2 [8, 17]. Some authors suggest to do away with such questions by arguing the constant K to be devoid of a clearly defined physical meaning for the streamer mechanism and hence necessarily of purely empirical character [18]. In [16] it is shown, however, that even when the the pressure and gap distance as well as the statistical nature of the single avalanche growth are considered in the calculation of PDIVs within the single-avalanche streamer theory, the results are still incompatible with the observed PDIVs in wedge-shaped air gaps bounded by dielectric coatings.

The more obvious way out of the disagreement between theory and experimental results would be to abandon the single-avalanche streamer mechanism as the appropriate theory 'behind' the constant K for calculating (partial) breakdown thresholds in quasi-uniform, atmospheric pressure air gaps, at least up to the centimeter gap spacing range. As indicated in the designation of the criterion (1), the assumption of a fundamentally different mechanism (Townsend mechanism), which is based on secondary avalanches initiated at the cathode by feedback from the primary avalanche [10], formally leads to the same sparking criterion in quasi-uniform fields. The streamer constant is then replaced by the natural logarithm of the inverse of the secondary electron feedback coefficient γ, which is defined as the average amount of secondary electrons emitted per ionization event in the primary avalanche:

$$\int \alpha_{\text{eff}} \cdot \mathrm{d}l \stackrel{!}{=} \ln\left(\gamma^{-1}\right). \tag{2}$$

This would also 'solve' the problem of the low value of the streamer constant ($K \approx 5..7$) which is needed to accurately predict the PDIV in typical twisted pair geometries (figure 1) [8, 17], because γ^{-1} can in principle take any value $\gtrsim 1$ in quasi-uniform configurations. However, a number of arguments have been raised against the validity of the Townsend mechanism for partial breakdown in dielectric-bounded gas gaps. The raised objections will be discussed in detail in section 5 in light of the results presented in sections 3 and 4. Suffice it here to list the questions raised against a multi-avalanche generation (Townsend) mechanism:

- Can secondary electrons be liberated efficiently from the dielectric cathode? [17, 19, 20]
- Is the Townsend criterion valid in the slightly non-uniform electric field occurring in configurations of the type shown in figure 1(a)? [17, 19–21]
- Can a Townsend discharge generate a sufficient discharge current magnitude (i.e. measureable by standard PD measurement techniques) before the discharge is quenched by charge deposition on the insulating coatings? [22]
- How can formative times and PD pulse current durations of some 10 ns be explained in a multi-avalanche theory?

The goal of this work is to present and validate a multi-avalanche discharge inception theory for quasi-uniform gas gaps in general (figure 1(c)) and wedge-shaped gas gaps in particular (figure 1(a)), which aims to address all of the raised concerns against such a multi-avalanche inception mechanism. The present paper deals with the determination of the *static inception threshold* of such configurations by proposing a physically motivated parametrization of the secondary electron emission coefficient γ that is based on the photoelectric effect at the (dielectric) cathode and the ion-enhanced field emission of electrons from the (dielectric) cathode. The theory is applied to the twisted pair geometry (figure 1(a)) and validated against a large body of literature data and own measurements. A subsequent publication will address the *dynamics* of the discharge mechanism, which is relevant for calculating breakdown probabilities under transient voltages, as well as for clarifying the above-mentioned questions about the formative time of the Townsend discharge and the magnitude of the discharge current.

2. Short historical overview on the development of breakdown criteria

In the vast literature devoted to the discussion of the static sparking threshold, there is a general agreement on the *mathematical form* of the static breakdown criterion. It was formulated in its generalized form shown in equation (1) as early as 1923 by Schumann [9]. In Schumann's formulation, which considers both positively and negatively charged particles to ionize with respective ionization coefficients β and α, the constant K is given by $\frac{\ln(k)}{1-1/k}$, where $k=\alpha/\beta$ is the ratio of the impact ionization coefficients. While direct impact ionization by positive ions is negligible with respect to impact ionization by electrons ($\beta \ll \alpha$), the consideration of secondary electron generation at the cathode by positive ions (γ_i mechanism), energetic photons (γ_{ph} mechanism) and other mechanisms lead to essentially indistinguishable functional parametrizations of the sparking criterion. The assumption of e.g. ionic feedback relates $\beta=\alpha\cdot\gamma_i$ to the secondary electron emission coefficient γ_i. For $\gamma_i \ll 1$, this leads to $K\approx\ln({\gamma_i}^{-1})$, which yields the Townsend criterion (2) for the static breakdown voltage. As its name suggests, it had already been formulated in the pioneering works of Townsend [10] and Thomson [2] in the first decade of the 20th century, albeit with the same misconception of seeing impact ionization of positive ions as the predominant electron supply mechanism. Schumann derives the values of K for a given parametrization of $\alpha(E)$ by comparing measured breakdown voltages with the model's predictions. He chose this semi-empirical approach because the value of K (and hence the derived sparking threshold) depends on the value of β, whose value was not known accurately, not least because of the missing understanding of the various cathode processes implicitly subsumed under the parameter β. The empirically derived values of K range from about 8 to 23 for atmospheric pressure air gaps ranging from $d=0.1$ cm to 1 cm. From today's perspective, this amounts to an estimation of the effective secondary electron feedback coefficient as a function of the gap width (electric field), as discussed below in section 3.2.

Another seminal contribution to the understanding of gas breakdown was the description and experimental study of the single-avalanche streamer breakdown mechanism during the late 1930s [11, 12]. This type of breakdown is characterized by the direct transformation of a single primary avalanche into a weakly-ionized plasma channel connecting the electrodes. Its characterizing feature is the supply of secondary avalanches originating in the gas phase, whose electron yield is enhanced by the space charge electric field created by the avalanche itself. This mechanism is observed under conditions where the Townsend mechanism is suppressed dynamically by using voltages with short rise times to bring the gap to a large overvoltage before the Townsend mechanism is able to become operative [12] or configurationally by having a low γ value (intrinsically low secondary electron yield, nonuniform fields, large gap spacings, etc). The latter has been hypothesized to apply for dielectric-bounded gas gaps by some authors, as discussed in section 5. As mentioned above, the associated simplified breakdown criterion (1) also takes the Schumann-type mathematical form with another physical model behind the constant K (see equation (33) in appendix I), and with physically motivated values ranging from about 14 to 20, depending on gas parameter and electric field values [12, 16, 23].

3. Theory

3.1. Approximate reduction of arbitrary quasi-uniform electrode configurations into parallel connected discharge cells

A quasi-uniform electrode configuration may be approximated as a parallel connection of uniform *discharge cells* (figure 1(b)). Assuming the dielectric coating to be of uniform thickness s and described by its complex relative permittivity $\underline{\varepsilon}_{\mathrm{r}}$, a discharge cell is fully characterized by its gap width d_i and its associated cathode surface area $A_{\mathrm{c},i}$. Any quasi-uniform electrode configuration is then approximatively reduced to a set of N_{c} tuples $\{(d_i,A_{\mathrm{c},i})|i=1,\ldots,N_{\mathrm{c}}\}$, where N_{c} is the chosen number of discharge cells. An adequate value of N_{c} is obtained by a mesh convergence study analogous to other discrete numerical schemes. The electrode area is not relevant for calculating the static breakdown threshold, which is why in this paper only the gap distance $d(x)$ parametrized by the continuous variable x will be used (see figure 1). The variable x is the ordinate of the point where the field line crosses the horizontal axis (cylindrical or rotational symmetry is assumed

for simplicity, but the concept of discharge cells is applicable to any geometry). The function $d(x)$ obviously depends on the investigated electrode geometry—an example of a simple approximate parametrization for contacting spheres or cylinders with insulating coatings in the limit $s \ll D$ is given in appendix A. The associated voltages in the gas gaps are given by the quasi-uniform approximation (capacitive voltage division between the gaseous and solid dielectric),

$$U_\mathrm{g}(x) = \frac{U_\mathrm{el}}{\left|1 + \frac{2s}{\underline{\varepsilon}_\mathrm{r} \cdot d(x)}\right|}, \tag{3}$$

and the average electric field along the field line reads

$$E_\mathrm{g}(x) = \frac{U_\mathrm{g}(x)}{d(x)} = \frac{U_\mathrm{el}}{\left|d(x) + \frac{2s}{\underline{\varepsilon}_\mathrm{r}}\right|}. \tag{4}$$

The (partial) breakdown threshold of the whole configuration is simply given by the lowest electrode voltage for which at least one of the gas gaps exceeds its corresponding breakdown electric field $E_\mathrm{b}(d(x))$:

$$U_\mathrm{el,b} = \min_{x \in [0,\infty)} E_\mathrm{b}(d(x)) \cdot \left|d(x) + \frac{2s}{\underline{\varepsilon}_\mathrm{r}}\right|. \tag{5}$$

A partial breakdown is obtained in the presence of an insulating coating, $s > 0$, in which case $U_\mathrm{el,b}$ is called the PDIV. In low-loss dielectric materials, $\underline{\varepsilon}_\mathrm{r} = \varepsilon_\mathrm{r}' - j \cdot \varepsilon_\mathrm{r}'' \approx \varepsilon_\mathrm{r}'$ and thus

$$\mathrm{PDIV} = \min_{x \in [0,\infty)} E_\mathrm{b}(d(x)) \cdot \left(d(x) + \frac{2s}{\varepsilon_\mathrm{r}'}\right). \tag{6}$$

The breakdown electric field E_b as a function of gap distance d was determined from own measurements as well as an extensive compilation of measured breakdown voltages of quasi-uniform gas gaps with metallic electrodes in atmospheric pressure air [9, 24–27]. The following parametrization is obtained:

$$E_\mathrm{b}(d) = \min\left(\mathrm{e}^{f(\ln(d/\mathrm{m}))}\,\mathrm{V \cdot m^{-1}}, E_\mathrm{FE}\right), \quad (1\,\mu\mathrm{m} < d \leqslant 10\,\mathrm{cm}) \tag{7}$$

where f is the polynomial

$$f(x) = 1.460 \cdot 10^{1} - 1.245 \cdot 10^{-1} \cdot x - 2.3055 \cdot 10^{-2} \cdot \times x^2 - 2.935 \cdot 10^{-3} \cdot x^3 \tag{8}$$

and $E_\mathrm{FE} = 82\ \mathrm{kV \cdot mm^{-1}}$ is a measured threshold value [28] that characterizes the transition to the field-emission (FE) controlled breakdown mechanism (with typical values ranging from $50\ \mathrm{kV \cdot mm^{-1}}$ to $150\ \mathrm{kV \cdot mm^{-1}}$ depending on the characterstics of the cathode surface [29]). In the FE-controlled mechanism, electron multiplication by impact ionization in the gas is no longer relevant. In large gaps, the above parametrization is validated by measured data up to $d = 10$ cm, above which the breakdown field will level off further from $E_\mathrm{b}(10\,\mathrm{cm}) = 2.67\ \mathrm{kV \cdot mm^{-1}}$ towards $E_\mathrm{crit} = 2.37\ \mathrm{kV \cdot mm^{-1}}$ [30].

The validity of the quasi-uniform approximation, equations (3) and (4), is investigated in appendix B for the example of contacting enameled wires of a total diameter of 1 mm and a coating thickness of $s = 30\ \mu$m. The difference in calculated PDIVs obtained by the full numerical field calculation and integration as compared to the simple uniform approximation with geometric field line length determination is less than 3%. A parametric study shows that the approximation is valid down to a total wire diameter of about 0.3 mm (at atmospheric pressure), below which the discharge gradually moves out to the more non-uniform electric field region.

3.2. Ionization threshold and value of the secondary electron feedback coefficient

The Townsend criterion (equation (2)) and the single-avalanche streamer criterion (equation (1)) can be combined into a single threshold value for the *ionization integral* $I = \int_0^d \alpha_\mathrm{eff} \cdot \mathrm{d}l$, which for a quasi-uniform electric field reads

$$I \approx \alpha_\mathrm{eff} \cdot d \overset{!}{=} \ln\left[\min\left(\frac{\alpha_\mathrm{eff}}{\alpha} \cdot \gamma^{-1}, n_\mathrm{crit}\right)\right] \equiv K. \tag{9}$$

Note that for the multi-avalanche (Townsend) mechanism, the effect of electron attachment is added here by the factor $\alpha_\mathrm{eff}/\alpha$, which equals the probability of non-attachment of a seed electron and is significantly smaller than 1 only in attaching gases near to the critical field value [16, 31]. The static breakdown electric field E_b is the electric field value satisfying the above equation, and $U_\mathrm{b} = E_\mathrm{b} \cdot d$ is the associated static breakdown voltage. The corresponding value of the ionization integral is called the *ionization threshold* and denoted $K = \alpha_\mathrm{eff}(E_\mathrm{b}) \cdot d$. Figure 2 shows the ionization thresholds corresponding to measured static breakdown voltages for atmospheric pressure air over a large range of gap distances. The shaded regions demarcate the ionization threshold range that would have been obtained for breakdown voltages deviating by $\pm 5\%$ and $\pm 10\%$, respectively, from the measured values. Conversely, the corresponding range indicates the error on the calculated breakdown voltage resulting from the use of a 'wrong' threshold value. For example, using $K = 18$ (dashed horizontal line) leads to a reasonable accuracy ($\pm 10\%$) on the calculated static breakdown voltages for gap distances of some mm to cm. On the other hand, the smaller the gap, the more sensitive the calculated breakdown voltage is to changes in the chosen ionization threshold K, and using the conventional streamer threshold (even if corrected for the effect of gap electric field as shown by the continuous black line [16]) will grossly overestimate the inception threshold. Yet, the range $d < 0.1$ mm is just the range that is relevant for PD inception in wedge-shaped gas gaps (see dashed blue d_min line in figure 5). This would explain why the streamer threshold, which is obtained by requiring a single avalanche to significantly distort the electrode field, and which works with reasonable accuracy for larger gaps, is not even approximatively applicable in this case. On the other hand, the small values of the modified 'streamer constants' (appropriate designation: ionization thresholds) for the calculation of PD inception voltages in wedge-shaped gas gaps (e.g. $K \approx 6$ for $d_\mathrm{min} \approx 50\ \mu$m in [17], $K \approx 5$ for $d_\mathrm{min} \approx 20\ \mu$m in [8]) agree very well

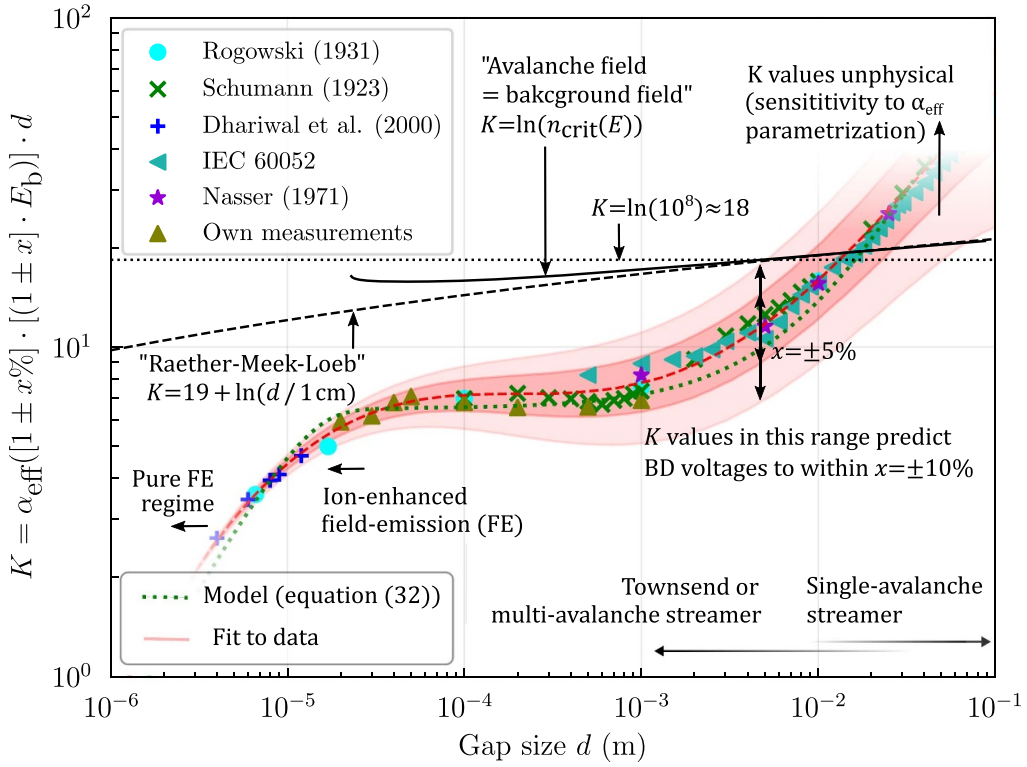

Figure 2. Critical ionization thresholds $K = \alpha_{\text{eff}}(E_\text{b}) \cdot d$ in atmospheric pressure air as a function of gap distance, calculated from measured breakdown voltages referenced in the the legend. The dashed red line is a fit to the shown experimental data. The K-values in the colored bands predict the breakdown strength to within $\pm5\%$ and $\pm10\%$, respectively. The green dotted line is a physically motivated parametrization $K = \ln(\gamma^{-1})$ in terms of the secondary electron emission coefficient given in equation (10).

with the values shown in figure 2 for the corresponding gap widths.

4. Results

4.1. Expected transition between breakdown modes for static breakdown

The data shown in figure 2 indicates that one should expect a transition from the Townsend to the single-avalanche streamer mechanism for static breakdown (i.e. without significant overvoltage) as the gap distance exceeds about 1 cm to 2 cm. However, the determined values of K (or γ) do not saturate at the expected streamer limit of $K \gtrsim 18$ ($\gamma \lesssim 10^{-8}$). As pointed out in the introduction, values of $K > 23$ (an average amount of $>10^{10}$ electrons in the avalanche head) are not physically meaningful, because the the effect of the space charge electric field of the avalanche on the ionization dynamics in the gap cannot be neglected in this regime. The reason for the excursion of the determined ionization threshold to large values $K \gg 23$ (instead of the expected saturation) in cm-sized gaps lies in its large sensitivity to the used $\alpha_{\text{eff}}(E)$ parametrization. As illustrated in appendix C, the applied parametrization from BOLSIG+ with the detachment correction from [32] seems to overestimate the net ionization rate in low electric fields ($2\ \text{kV}\cdot\text{mm}^{-1} < E < 3\ \text{kV}\cdot\text{mm}^{-1}$). This leads to a lower critical field value ($\sim$2.2 $\text{kV}\cdot\text{mm}^{-1}$) than measured experimentally ($\sim$2.37 $\text{kV}\cdot\text{mm}^{-1}$ [30]), and thus large relative differences in the calculated values of the ionization thresholds in cm-sized gaps.

The activation of the single-avalanche streamer mechanism is thus expected in cm-sized gaps, and explained within the model described in section 3.2 by the increasing difficulty for photons to reach the cathode due to their increased absorption in the gas in larger gaps. The average number of electrons in the single avalanche at the breakdown electric field thus increases with increasing gap size, until it reaches streamer-forming proportions. As discussed in appendix H, the feedback of photoelectrically active photons to the cathode in atmospheric pressure air gaps longer than about 2 cm is effectively stifled ($\alpha_{\text{eff}} \approx \eta_{\text{ph}}$), and hence photo-ionization in the gas gradually gains in importance as the gap distance approaches this value. Thus, a rather seamless transition from the Townsend to the single-avalanche streamer mechanism would indeed be expected around 2 cm, which is in line with experimental observations [33].

4.2. Physical parametrization of the secondary electron feedback coefficient

In appendix H the following parametrization of the secondary electron emission coefficient is motivated:

$$\gamma = \gamma_{\text{ph}} \cdot \frac{1}{1-\frac{\eta_{\text{ph}}}{\alpha_{\text{eff}}}} \cdot \mathrm{e}^{-\eta_{\text{ph}}\cdot d} + \gamma_{\text{FE}} \cdot \mathrm{e}^{-\frac{D}{E}}. \tag{10}$$

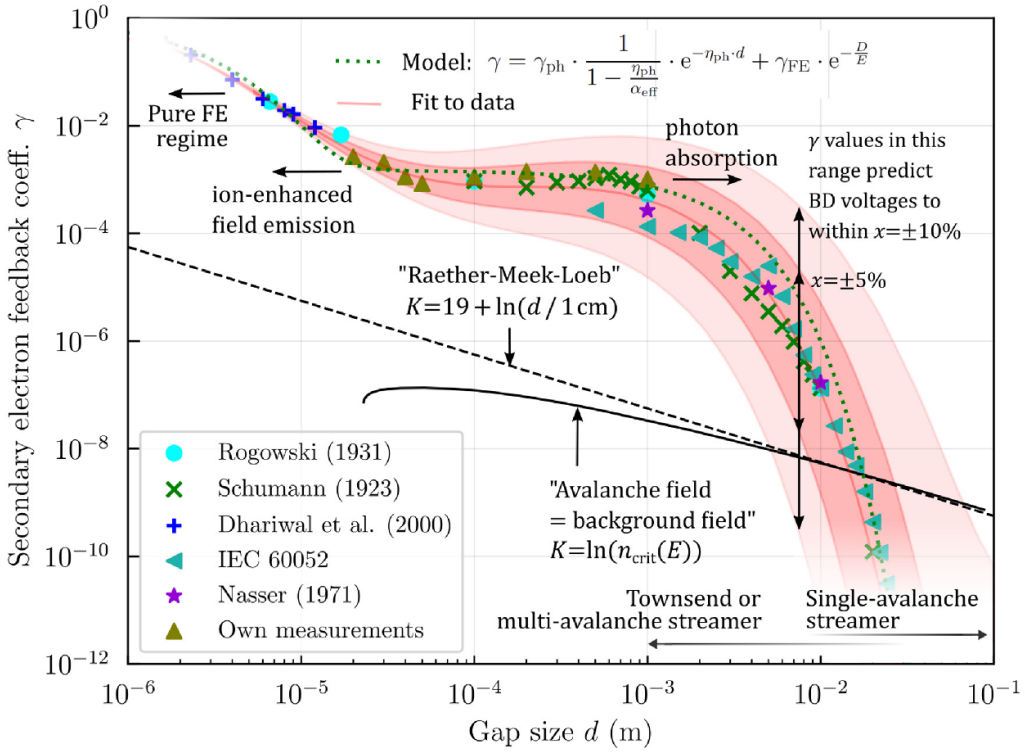

Figure 3. Derived values of the (effective) secondary electron emission coefficient in dry atmospheric pressure air as a function of gap distance for metallic electrodes by using measured breakdown voltages from the indicated references. The green dotted line is a physically motivated parametrization (see section 4.2) based on photon feedback ($\gamma_{ph} = 1.5 \cdot 10^{-3}$) with absorption in the atmospheric pressure air ($\eta_{ph} = 8$ cm^{-1}) and ion-enhanced field emission of secondary electrons ($\gamma_{FE} = 0.9$). In this model, photon absorption explains the sharp drop of γ in larger gaps ($d > 1$ mm), while the strong increase below about $d = 30$ μm is due to the activation of ion-enhanced field emission by the large electric field values reached in small gaps before breakdown.

The first term is a contribution from energetic photons freeing electrons by photoelectric effect at the (dielectric) cathode, with consideration of the absorption of photons by the gas molecules (transformation of photon energy into non-radiative channels or low-energy photons). The second term is activated only in large electric fields (small gap widths), and describes an ion-enhanced field emission process [34].

The values of the coefficients for the plotted line in figure 3 are $\gamma_{ph} = 1.5 \cdot 10^{-3}$ and $\gamma_{FE} = 0.9$. The value $\eta_{ph} = 8$ cm^{-1} of the effective absorption coefficient is in reasonable agreement with the value of ∼5 cm^{-1} applying to the absorption of photoionizing radiation from a corona discharge in dry air [35]. The parameter $D = 178$ kV · mm^{-1}, which characterizes the field-emission onset threshold, is taken from [36]. This threshold value predicts the onset of the ion-enhanced FE regime very well (increase of γ below a gap width of ∼30 μm, see figure 3).

4.3. Parametrization of the static inception voltage

The Townsend threshold voltage U_T satisfying the criterion (2) with the secondary feedback γ from figure 3 is shown in figure 4 for a range of gas gap widths d and reduced coating thicknesses s/ε_r' (the variables s and ε_r' only appear as a ratio in the model). The corresponding geometry is shown in the upper-left corner. If the electrode voltage is below U_T, the probability of an avalanche chain growing to measureable proportions or even (partial) breakdown is negligible, whereas this probability increases rapidly when the electrode voltage exceeds U_T [16, 37].

Figure 4 also illustrates that for a given reduced coating thickness s/ε_r', there is a minimum threshold voltage $U_{T,min}$ at a specific gap width d_{min}. The corresponding minimum values are indicated by the dashed white line. For $s/\varepsilon_r' \to 0$, the value levels off to the Paschen minimum of atmospheric pressure air (∼340 V). Note, however, that the onset of a pure FE controlled mechanism (i.e. negligible electron multiplication in the gas) occurring in gap widths below about 7 μm in atmospheric pressure air allows these gaps to break down at voltages below the Paschen minimum (see equation (7)) [28, 29].

For $s/\varepsilon_r' > 0$, the threshold $U_{T,min}$ is larger than the Paschen minimum, because part of the electrode voltage drops across the solid dielectric. $U_{T,min}$ then corresponds to the PDIV of a wedge-shaped gas gap, such as the one shown in the lower-right corner. As mentioned in the previous paragraph, lower PDIVs can be obtained if the purely FE controlled breakdown mechanism is activated. The conditions under which this mechanism can occur are specified in the next section. The following section also contains an experimental validation of the PDIVs of wedge-shaped gas gaps in contacting enameled wires as a function of s/ε_r'.

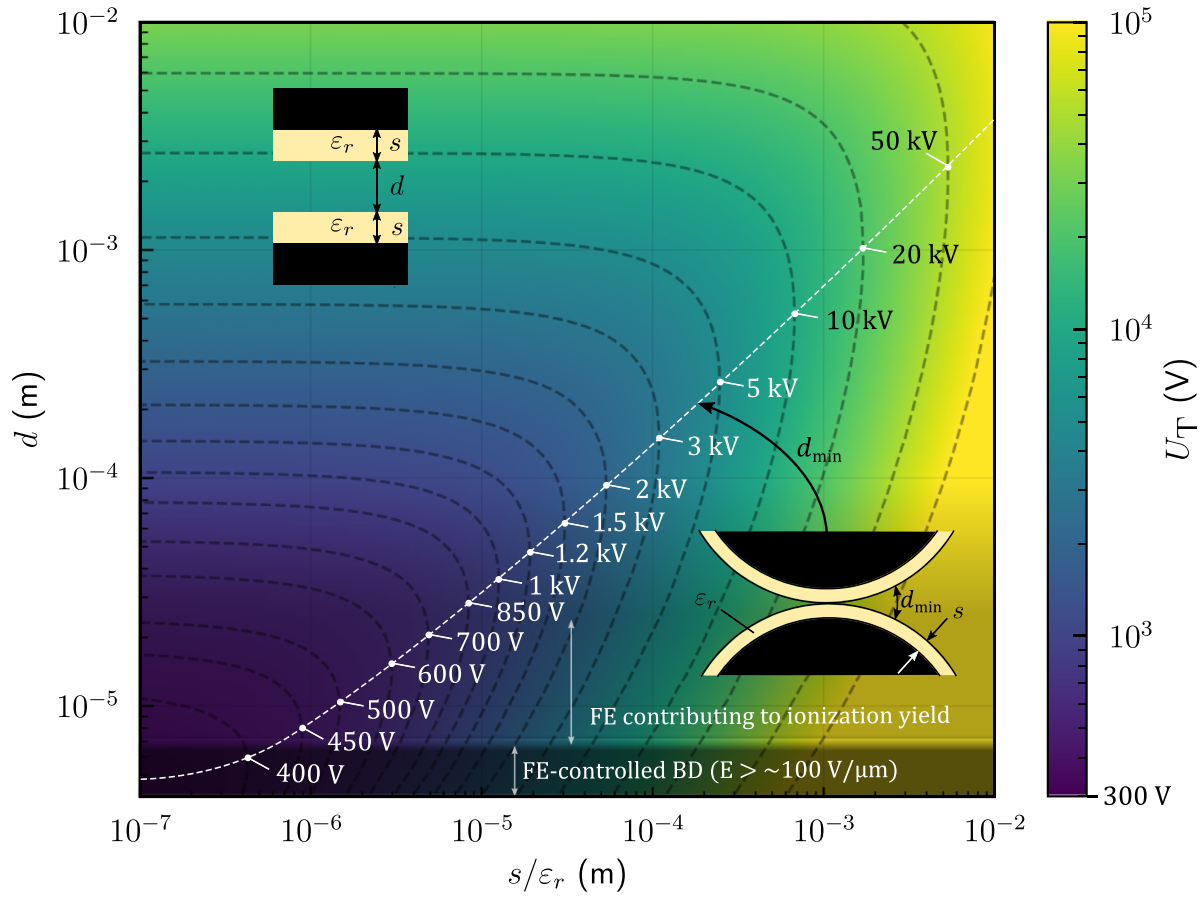

Figure 4. Minimum breakdown thresholds in dry atmospheric pressure air (in volts peak of electrode voltage) as a function of gas gap length d and the reduced dielectric layer thickness s/ε_r'. The color coding and the dashed iso-lines indicate the Townsend threshold voltage according to the criterion (2). The dashed white line indicates the minimum voltage $U_{T,min}$ at which a quasi-uniform wedge-shaped gap characterized by a certain s/ε_r' will fulfill the Townsend criterion (at the corresponding gap length d_{min}).

4.4. Case study: PDIV of contacting enameled wire pair

For quasi-uniform wedge-shaped gas gaps ($s/\varepsilon_r' > 0$, as illustrated in the lower-right corner of figure 4), the PDIV equals the lowest value of the Townsend thresholds of all the discharge cells, and is given by

$$\mathrm{PDIV}(s/\varepsilon_r') = U_{T,min}(s/\varepsilon_r') = \min_{d\in(0,\infty)} U_T(d, s/\varepsilon_r'). \quad (11)$$

Note that on the basis of the observation described in section 4.1, the Townsend criterion alone is used instead of the combined criterion (9).

The gap width of the discharge cell that incepts at the lowest voltage is a certain d_{min}. As mentioned in section 4.3, for very thin reduced coating thicknesses ($s/\varepsilon_r' \lesssim 1$ µm), the smallest gas gaps ($d \lesssim 7$ µm) can break down by a FE controlled mechanism below the minimum Townsend threshold. The corresponding (macroscopic) electric field threshold is estimated to lie between 50 kV · mm^{-1} and 150 kV · mm^{-1}, which is a typical order of magnitude for the measured onset field for FE-controlled breakdown in microscale gaps with metallic electrodes [28, 38]. Note, however, that FE starts to play a contributing role already in larger gaps below about 30 µm [34, 39] as explained in section 4.2 and appendix H.1. The discharge mechanism in these gaps is still a proper gas breakdown as opposed to the pure FE-regime ($E > E_{FE}$), where the presence of the gas molecules in the inter-electrode volume becomes negligible ($\rightarrow$ vacuum breakdown).

For better readability, the PDIV ($=$minimum Townsend threshold $U_{T,min}$) for wedge-shaped gas gaps characterized by the reduced coating thickness s/ε_r' is shown separately in figure 5 together with the associated gap length d_{min} at which breakdown can first occur. The threshold voltages for FE-controlled breakdown of gas gaps bounded by coatings with small s/ε_r' is shown for the theoretical limit $d \rightarrow 0$ as well as $d = 1$ µm and $d = 2$ µm.

A compilation of literature data of measured PDIV in wedge-shaped air gaps at atmospheric pressure is shown in figure 6 together with model predictions. It can be seen that the single-avalanche streamer criterion grossly overestimates the PDIV, while a commonly used value of the secondary feedback coefficient in atmospheric pressure air, $\gamma = 2.2 \cdot 10^{-4}$ [40], also overestimates the PDIV, albeit less drastically. A very satisfactory agreement with experimental data is obtained when the PDIV is calculated from the actual breakdown voltage values between metallic electrodes, which correspond to the ionization threshold (or effective secondary electron emission coefficient) shown in figure 2 (or figure 3). The data

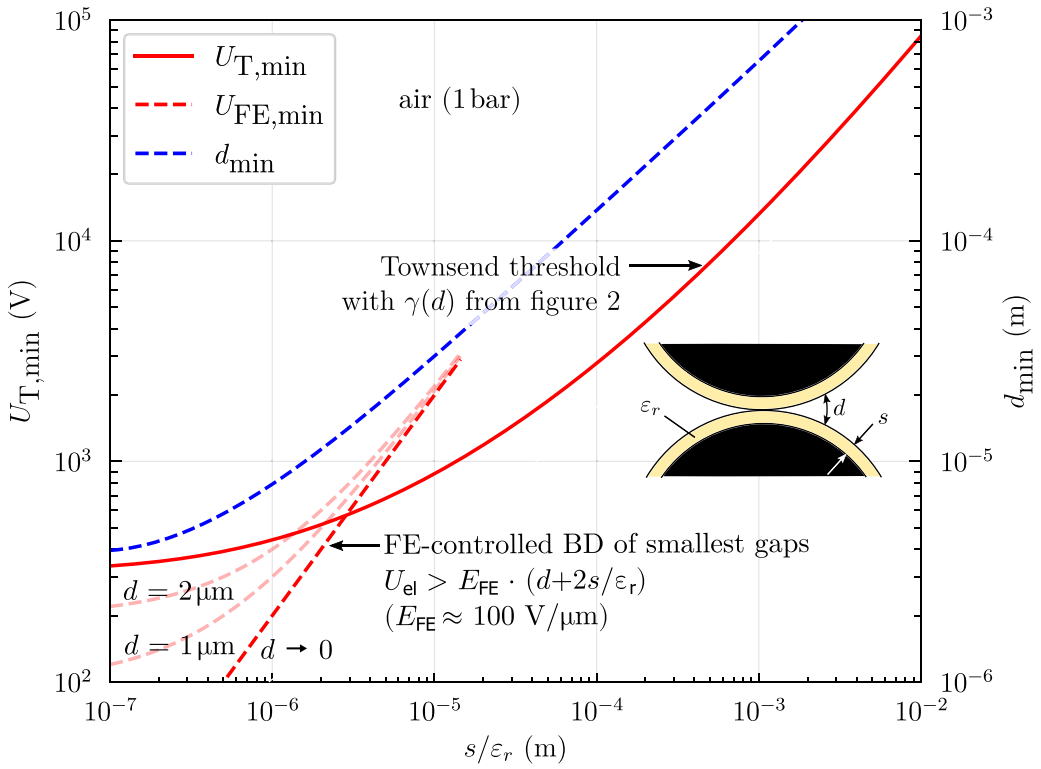

Figure 5. Minimum voltage $U_{T,min}$ for which the Townsend threshold is reached along the field line of length d_{min} within the wedge-shaped gas gap. With thin coatings, FE controlled breakdowns of the smallest gaps can occur below the Townsend threshold.

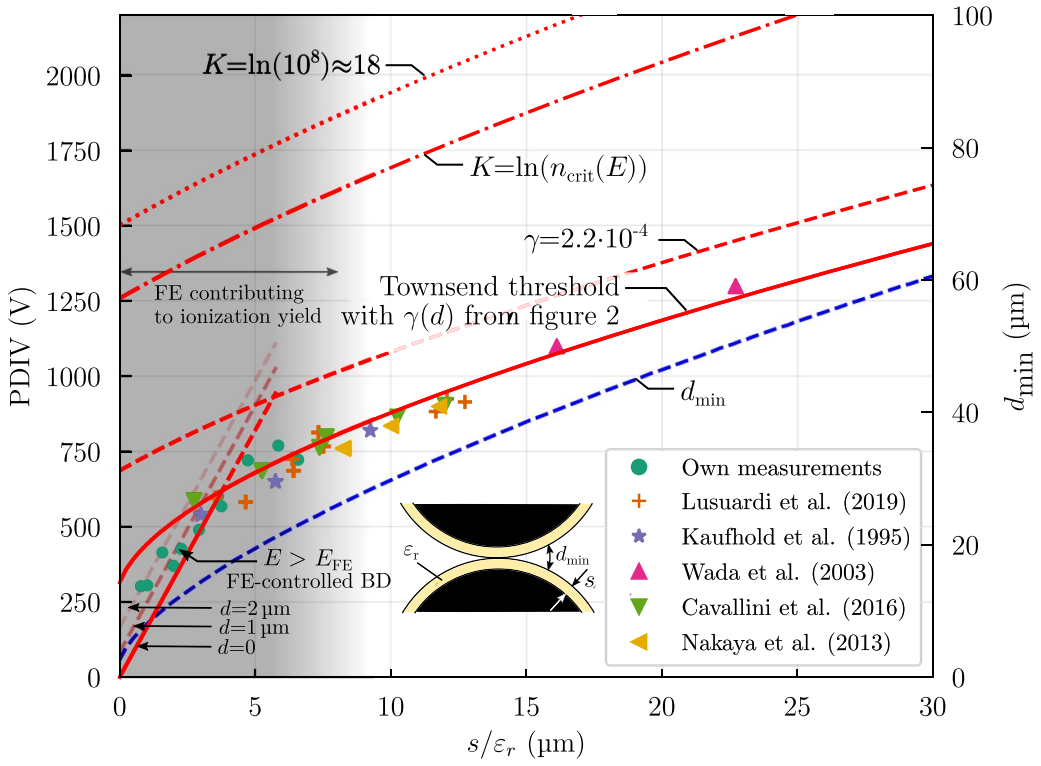

Figure 6. Comparison of various model predictions for PDIV in wedge-shaped air gaps (atmospheric pressure) as a function of the reduced coating thickness s/ε_r'. The length d_{min} of the gas gap breaking down at PDIV is indicated on the right vertical axis. The shaded region indicates where ion-enhanced FE is active according to the secondary feedback model shown in figure 3. The pure FE regime (delineated by the straight lines), in which the ionization dynamics in the gas is negligible, is activated below the Townsend threshold in wedge-shaped gaps with coatings of reduced thicknesses below a few micrometers.

points indicating the transition into the pure FE regime (green circles in figure 6) have been obtained by using sphere-plane ($R = 5$ mm) aluminum electrodes with an aluminum oxide layer (obtained by hard anodizing) with a thickness of $s \approx 50\,\mu$m as a dielectric coating. These coatings exhibit a dielectric permittivity increasing significantly with the air relative humidity, thus allowing to reach reduced coating thicknesses in the range from 7 μm (dry air) down to 1 μm in humid air (80% relative humidity at 25 °C, 1 kHz). Also, when the relative air humidity is not close to zero, the imaginary part of the permittivity can in general not be neglected in these coatings. Appendix E shows how to calculate an effective reduced coating thickness $(s/\varepsilon_\mathrm{r}')_\mathrm{eff}$, which takes into consideration both real and imaginary parts of the permittivity, and which allows to locate these data points on the horizontal axis in figure 6.

In practice, when the determination of the PDIV and not its parametrization in terms of a real (effective) reduced dielectric coating thickness is the main goal, the PDIV can be calculated most directly and without the restriction $\varepsilon_\mathrm{r}'' \ll \varepsilon_\mathrm{r}'$ by using equations (5) and (7):

$$\mathrm{PDIV}(s/\underline{\varepsilon}_\mathrm{r}) = \min_{d\in(0,\infty)} E_\mathrm{b}(d)\cdot\left|d+\frac{2s}{\underline{\varepsilon}_\mathrm{r}}\right|. \tag{12}$$

Note that the use of equation (12) in general leads to more accurate PDIV values than the use of equation (9) with the physical parametrization (10), because the latter slightly overestimates the value of K around $d = 20\,\mu$m, which is a relevant gap width for typical magnet wire configurations (see figure 6), and the PDIV depends more sensitively on the chosen value of K for these small gaps (see figure 2: the green dotted line touches the $\pm 10\%$ region around $d = 20\,\mu$m).

For ease of practical reference, the following polynomial fit to equation (12) is provided,

$$\frac{\mathrm{PDIV}(s/\varepsilon_\mathrm{r}')}{\mathrm{V}} = 4.64\cdot 10^2 + 4.66\cdot 10^1\cdot\frac{s/\varepsilon_\mathrm{r}'}{\mu\mathrm{m}} - 6.16\cdot 10^{-1}\cdot \times\left(\frac{s/\varepsilon_\mathrm{r}'}{\mu\mathrm{m}}\right)^2 + 5.08\cdot 10^{-1}\cdot\left(\frac{s/\varepsilon_\mathrm{r}'}{\mu\mathrm{m}}\right)^3 \tag{13}$$

which is accurate to within a relative error of $<1.3\%$ for $4\,\mu\mathrm{m} < s/\varepsilon_\mathrm{r}' < 50\,\mu$m.

5. Discussion

For breakdown inception in quasi-uniform atmospheric pressure air gaps under negligible overvoltage (static breakdown threshold), the presented analysis suggests the presence of a photon-assisted cathode feedback as the main source of secondary electrons driving the discharge development in gaps ranging from some dozens of micrometers to a few centimeters. Noticeable photon absorption starts for gaps $d \gtrsim 1$ mm and practically stifles this feedback process ($\gamma < 10^{-10}$) when the gap width reaches a few centimeters, where presumably secondary feedback from the *gas bulk* starts to dominate (streamer mechanism). Incidentally, note that a single-avalanche streamer mechanism is still possible in smaller gaps if a sufficient overvoltage is reached before the Townsend breakdown collapses the gap voltage [16]. The associated conditions on the rate of rise of the applied gap voltage as a function of relevant system parameters will be discussed in a follow-up paper which deals with the dynamical aspects of the multi-avalanche breakdown mechanism considered here.

As mentioned in the introduction, a number of concerns have been raised against a multi-avalanche (Townsend) mechanism occurring in wedge-shaped gas gaps of the prototypical geometry shown in figure 1(a). The authors in [17] claim for example that the Townsend mechanism is not plausible 'since the emission of secondary electrons from the insulated cathode by positive ion or UV bombardment is extremely unlikely' because 'the work function of e.g. copper is 4–5 eV, whereas in an insulator it is 9 eV' (p 10). This concern seems to be unfounded, however, because according to [41], the measured work functions of typical insulating polymers lie between 4 eV–5.5 eV, which are very similar to the work functions of metals typically used as electrodes (aluminum, copper, brass, steel). Moreover, the average value $K \approx 6$, obtained in [17] as a good fit to the experimentally measured PDIVs in various wire geometries amounts to a critical amount of some $\mathrm{e}^K \approx 400$ avalanche electrons for the assumed avalanche-to-streamer transition. This is a questionable result, because no noticeable distortion of the background electric field is achieved with this small amount of electrons in the avalanche head [16]. Rather, this low number of electrons in the primary avalanche at breakdown points towards a multi-avalanche (Townsend) process as the initiating stage of a PD in the considered system.

Another common misconception is that the Townsend mechanism is only suitable to describe the 'onset of breakdown phenomena in uniform fields' (p 10) [17]. In fact, secondary feedback can be active even in strongly non-uniform electrode geometries, albeit with a position-dependent value of the secondary feedback coefficient [42], which drops off rapidly away from the cathode. In quasi-uniform fields, which are the focus of this work, the approximation of a position-independent γ value is found to be a valid approximation for the calculation of PDIVs in wedge-shaped gas gaps (as shown in section 4.4), and it leads to the form given in equation (2). In [21], the applicability of the uniform approximation $\int_0^d \alpha_\mathrm{eff}\cdot \mathrm{d}x \approx \alpha_\mathrm{eff}(U_\mathrm{g}/d)\cdot d$ is questioned for the twisted pair geometry (d is the length of the considered field line in the gas, and U_g the voltage across the gas gap). In the present paper, using the value of α_eff evaluated at the average electric field $U_\mathrm{g,uni}/d_\mathrm{geo}$, where $U_\mathrm{g,uni}$ is the gap voltage determined by means of the uniform field approximation (3) and d_geo is the field line length determined by the geometric approximation (14), was found to be accurate for all the investigated wire geometries taken from five different literature sources. This result questions the general need for numerical field simulation in dry air that is often employed for calculating the PDIV of contacting enameled wires (e.g. [17, 21, 43]). Also, it should be emphasized that the quasi-uniform approximation (3) has been used successfully by Halleck as early as 1956 to calculate the PDIV of twisted

wire samples [44], and is thus not to be regarded as an original contribution of this paper.

Another concern raised against the Townsend mechanism (or, rather, in favor of the single-avalanche streamer mechanism) is its seeming inability to incept discharges with currents of sufficient magnitude ($\geqslant$1 mA) in dielectric-bounded gas gaps [16]. In [22] the authors suggest that the streamer type PD is the discharge type which 'produces pulse charges of sufficient magnitude to be detectable by standard PD measurement techniques in technical equipment' (p 732). In this work we argue that the Townsend mechanism can *initiate* a PD of conventionally measureable pulse charge, if space-charge-assisted ionization is taken into account. An example of such an ionization mechanism known to be operative in metallic-bounded gas gaps [24] is the constriction of the electric field into the cathode fall by a space charge ionization wave consisting of positive ionic space charge deposited by many avalanche generations driven by fast photon secondary feedback. A more detailed account of this mechanism and a discussion of its sensitivity to the presence of the dielectric boundary will be given in the follow-up paper focusing on the dynamics of the discharge process. Moreover, the role of the dynamics of surface charges on the dielectric boundaries will be discussed.

Finally, the Townsend mechanism is commonly regarded as a 'slow' mechanism, because it forms over several avalanche generations. In contrast, streamer formation is fast, its formative time being mainly determined by the time required for a single avalanche to reach streamer forming properties, which is on the order of or less than the electron transit time in the gap [12, 16]. Breakdowns under transient voltages are observed to form with delay times as short as a few nanoseconds [4] (depending on the gap width and the amount of overvoltage), which leaves no time for positive ions generated by the primary avalanche to drift back to cathode and generate secondary electrons. This argument is still used in modern textbooks (e.g. [45], chapter 8.3.2) as part of the motivation for the 'fast' single-avalanche streamer breakdown mechanism, which does not depend on secondary electrons from the cathode, to explain formative times less than $\sim$100 ns in mm-sized quasi-uniform gaps. However, this line of reasoning loses its standing when the photoelectric effect at the cathode is considered as the main source of secondary electrons. Even if the associated formative time diverges as the overvoltage approaches zero, a photon-driven secondary feedback features a rapid drop of the formative time as a function of overvoltage, such that its value can reach 50 ns at only 10% overvoltage, as will be shown in the follow-up paper on the discharge dynamics.

Notwithstanding all these objections, the Townsend criterion has been previously used extensively to model the PDIV of wedge-shaped air gaps (e.g. [46–48]), even though the above concerns have not been addressed conclusively, if at all. Moreover, there is no agreement among reported values of the secondary electron emission coefficient γ, even for the same coating material [20, 21]. In fact, γ is mostly used as a 'fit factor', i.e. its value is chosen such as to obtain the best agreement with the measured PDIV. Because somewhat different γ values are obtained to best fit the PDIV of different wire geometries under different environmental conditions, the secondary electron emission coefficient is thus made to depend on these factors through the fitting procedure (for example γ as a function of temperature [21]). This is not to say that γ cannot in principle be a function of, e.g. temperature, but that often the actual physical mechanisms are not fully considered (e.g. the change of ε_r' with temperature in [21]), and the temperature dependence is then—at least in part—misattributed to the secondary electron emission coefficient. This strongly reduces the predictive power of the model, because it is not quite clear which value should be used *a priori* for a new insulation configuration and environmental condition. Furthermore, there is generally no clear picture of the physical processes behind the observed variation of γ with various system parameters. It is hoped that the physical parametrization of the secondary electron emission coefficient γ suggested in this paper will help to distinguish more clearly in the future between actual physical influences on γ, and influences merely enforced on γ by its use as a 'fit factor'.

From the scatter of the measured data points in figure 6 it can be inferred that the measurement of the PDIV of a wedge-shaped air gap is itself associated with a non-negligible measurement uncertainty. Possible reasons for this variation include the different sensitivities of the employed PD instruments, inaccuracies in the determination of the coating thickness and the dielectric permittivity as well as possible small differences in the ambient conditions (e.g. 'atmospheric pressure' is usually not controlled to the standard atmosphere of 1013.25 mbar, or the amount of air humidity may vary between investigators). Thus, although the approximations used in this paper (quasi-uniform electric field, using E_b from metallic electrodes for dielectric boundaries) necessarily introduce a certain error, this error should be compared to the practically achievable measurement accuracy. This is the meaning behind the term 'valid approximation' used in this paper.

Finally, it can be argued that while the parametrization (10) provides useful insight into the physics of the discharge process, the use of a breakdown criterion of the form $\alpha_{\mathrm{eff}} \cdot d = K = \ln(\gamma^{-1})$ for the determination of PDIVs in wedge-shaped gas gaps is unnecessarily complicated compared to a direct equation of the form (12). This conclusion is further supported by the observation presented in this paper that the values of the secondary electron emission coefficient derived from breakdown measurements with *metallic* electrodes lead to accurate predictions of the PDIV in gaps with *dielectric* boundaries. This suggests, in line with the above-cited literature values, that indeed the work functions for metals and polymers are not in general significantly different, such that secondary electrons can be liberated with a similar yield from both substrates (similar values of γ_{ph} and γ_{FE}).

More fundamentally, it is emphasized in this paper (appendix C) that using the ionization coefficient for describing the avalanche development in typical enameled wire geometries may still be reasonably accurate at atmospheric pressure, but most likely not in partial vacuum, which is an important application case for PDIV modeling in the context of more-electric aircraft [49]. This again suggests the use of experimentally determined breakdown electric fields

$E_b(d)$ between metallic electrodes in combination with an equation of the type (12) for determining the PDIV of wedge-shaped gas gaps. For the ambient conditions investigated in this paper (atmospheric pressure air at room temperature), the breakdown electric field measured between metallic electrodes under the same conditions was found to predict the PDIV in wedge-shaped, dielectric-bounded gas gaps accurately in combination with the quasi-uniform approximation for the gap electric field. It will be interesting to investigate if the same holds true when the ambient conditions are varied within the full range relevant for practical applications (e.g. pressure <1 bar, temperature >25 °C, low or high air humidity). In its present form, the model presented in this paper considers such variations of ambient conditions through the Paschen substitution $d \to N \cdot d$ (with $N = p/k_B T$) in the function E_b, as well as their influence on the value of the reduced coating thickness (expected by their influence on the dielectric permittivity $\underline{\varepsilon}_r = \underline{\varepsilon}_r(T, RH)$). Future work will thus be dedicated to determine the limits of the presented model, and find suitable extensions where needed.

6. Conclusion

A physically motivated parametrization of the secondary electron emission coefficient γ for atmospheric pressure air is suggested based on the observed variation of γ with gap width. Within this model, the secondary emission of electrons is mainly attributed to the photoelectric effect at the dielectric cathode, with an additional contribution due to ion-enhanced FE in small gaps ($d \lesssim 30$ μm). The associated Townsend theory of breakdown is able to predict in a satisfactory manner the measured PDIVs of twisted enameled wire pairs as a function of a single parameter, namely the reduced coating thickness $s/\underline{\varepsilon}_r$ of the insulating layer. Moreover, the paper advocates a more straightforward way of calculating the PDIVs of wedge-shaped gas gaps bounded by dielectric barriers, forgoing the use of the breakdown criteria based on the ionization integral (ionization coefficient), as well as numerical field simulations. This approach is applicable within the quasi-uniform field approximation, which is shown to be sufficiently accurate for the vast majority of practical enameled wire geometries. Future investigations will focus on the extension of the proposed model to the full range of ambient conditions relevant in practical applications.

Data availability statement

All data that support the findings of this study are included within the article (and any supplementary files).

Appendix A. Approximate calculation of the field line length

In the quasi-uniform approximation, the field line length d is irrelevant for the calculation of the PDIV of wedge-shaped air gaps starting from a contact point $d = 0$, because d is simply the parameter which is varied to find the minimum in expression (12). It might however be interesting to estimate the discharge location on the horizontal axis (see figure 7). In this case, a relationship between the horizontal axis coordinate x and the field line length is required. A simple approach consists in approximating the field line length by the length of the vertical line connecting the start and end of the field line in the gas. A small exercise in trigonometry leads to the following expression:

$$d(x) \approx d_{geo}(x) = \frac{x^2}{R+s}. \tag{14}$$

The accuracy of this approximation is demonstrated in figure 7, where the value of the ionization integral is calculated with both the actual field line length d_{num} from the numerical field simulation and the approximation (14). The next higher-order goemetric approximation (approximating the field line length with two line segments of equal length) does not significantly increase the accuracy of the predicted PDIV.

Appendix B. Influence of the electric field non-uniformity on the calculated ionization threshold

The simplicity of the parametrization of the PDIV on the sole parameter s/ε_r' relies on the validity of the 'parallel-plate capacitor approximation' of the inter-electrode space (figure 1). It consists in approximating the ionization integral using the numerical solution $E(x)$ of the Laplace equation,

$$\int_0^d \alpha_{eff}(E(x)) \cdot \mathrm{d}x, \tag{15}$$

(integration along a field line of length d in the gas gap) by the analytical solution for a parallel-plate capacitor,

$$\alpha_{eff}\left(\frac{U_{el}}{d + \frac{2s}{\varepsilon_r'}}\right) \cdot d. \tag{16}$$

The accuracy of this approximation is quantified on the example of a typical wire geometry, with a total wire diameter of $D = 1$ mm, a coating thickness of $s = 30$ μm and a dielectric permittivity of $\varepsilon_r' = 4.1$ (example wire W6 from [17]). The difference in calculated PDIVs with the two equations (15) and (16) is less than 3%. The approximation thus is adequate except for very thin wires ($D + s \lesssim 0.3$ mm), for which the discharge will be displaced outwards into the more non-uniform electric field region.

Appendix C. The impact of the choice of α_{eff} on the value of the ionization threshold

For calculating the ionization thresholds $\alpha_{eff}(U_b/d) \cdot d$ shown in figure 2, a parametrization of α_{eff} in terms of the electric field E is required. Depending on the underlying measurement data and the assumptions in the data analysis, different parametrizations of α_{eff} have been suggested in the

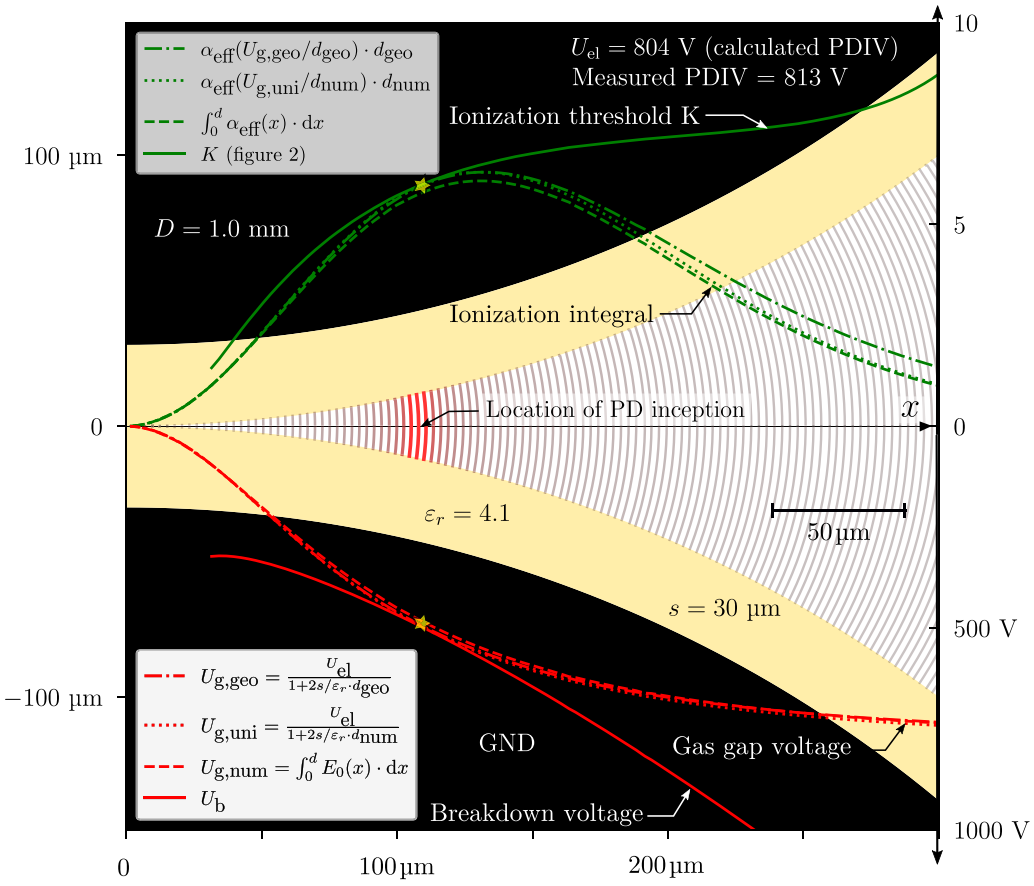

Figure 7. Investigation of the influence of the electric field non-uniformity in a wedge-shaped air gap on the employed approximations for the ionization integral (top) and the gas gap voltage (bottom).

literature. How much the choice of the parametrization α_{eff} affects the determined value of K is a relevant question. This is especially true for the large electric fields ($>10\,\mathrm{kV \cdot mm^{-1}}$) occurring in the wedge-shaped air gaps of magnet wires, for which measurement data and corresponding parametrizations of α_{eff} are scarce. Figure 8(a) compares the effective ionization coefficient for synthetic air (79% N_2, 21% O_2) as obtained from the Boltzmann solver BOLSIG+ [50] based on the cross section data of the SIGLO data base [51] with measured data [30, 52–54]. The fit line through the measured data is given by

$$\alpha_{\mathrm{eff}}(E) = c_1 \cdot \mathrm{e}^{-\frac{E_{\mathrm{th}}}{E}} + c_2 \cdot E - c_3 \cdot \mathrm{e}^{-\frac{E-E_{\mathrm{crit}}}{E''_{\mathrm{th}}}} \qquad (17)$$

with $c_1 = 910\ \mathrm{mm^{-1}}$, $c_2 = 23\ \mathrm{mm \cdot kV^{-1}}$, $c_3 = 6338\ \mathrm{mm^{-1}}$, $E''_{\mathrm{th}} = 50\ \ \mathrm{kV \cdot mm^{-1}}$, $E_{\mathrm{th}} = 25.5\ \ \mathrm{kV \cdot mm^{-1}}$ and $E_{\mathrm{crit}} = 2.42\ \mathrm{kV \cdot mm^{-1}}$.

It is important to emphasize that the ionization threshold derived from measured breakdown voltages depends on the employed $\alpha_{\mathrm{eff}}(E)$ parametrization. For gap widths below about 0.1 mm, using different parametrizations with a given ionization threshold will lead to significantly different calculated breakdown voltages. This point is illustrated in figure 8(b), which shows the derived ionization thresholds for the two $\alpha_{\mathrm{eff}}(E)$ parametrizations shown in figure 8(a) (the shaded regions indicate the range leading to breakdown voltages with a relative deviation of ±5%). While the conclusions about the underlying physical processes giving the curves their characteristic shape (results presented in section 3.2) remain valid in both cases, using one ionization threshold with the non-associated $\alpha_{\mathrm{eff}}(E)$ parametrization would lead to breakdown values significantly deviating from the measured values for $d \lesssim 1$ mm. This observation further supports—in addition to its practical straighforwardness—the use of a more direct equation such as (12) for determining the PDIV of wedge-shaped gas gaps, instead of making the detour via the ionization threshold. Nevertheless, from a more theoretical perspective, the physical insights derived from the analysis of $K(d)$ (or $\gamma(d)$) are valuable hints for understanding the basic phenomena involved in the breakdown process.

For cm-sized gaps, the situation is reversed. The exact value of the chosen ionization threshold has a comparatively small impact on the calculated breakdown voltage. On the other hand, the inverse process, i.e. the calculation of ionization thresholds from measured breakdown voltages and an α_{eff} parametrization, depends very sensitively on these input values. This is also illustrated in figure 8(b), where the ionization thresholds for slightly different parametrizations as well as the ±5% variation of the breakdown voltage cover a large range of values in the $d \gtrsim 1$ cm, including unphysical values $K \gtrsim 23$. The unphysical values do for example not

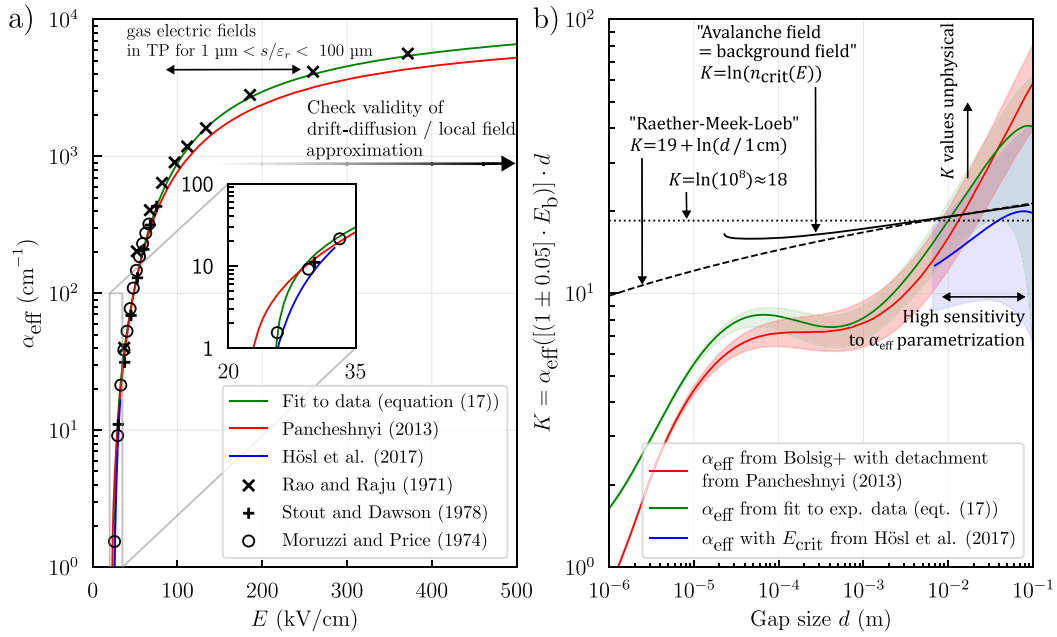

Figure 8. (a) Comparison of different parametrizations of the effective ionization coefficient. (b) Derived shape of the ionization threshold on the basis of the three α_{eff} parametrizations shown in subfigure (a).

occur with the shown quadratic low-field approximation $\alpha_{\text{eff}}(E) = \text{k} \cdot (E - E_{\text{crit}})^2$, where $k = 2.1\ \text{mm} \cdot \text{kV}^{-1}$ [55] and $E_{\text{crit}} = (2.37)\ \text{kV} \cdot \text{mm}^{-1}$ [30].

Another aspect that has not been examined in detail for the calculation of PDIVs in twisted pair geometries is the following. When using the ionization coefficient, the electron dynamics is implicitly assumed to be described within the drift-diffusion approximation of electron transport in the gas, and hence its limitations apply. The gas must be only weakly ionized, and the plasma must be collisional, i.e. the mean free path of elastic electron-neutral collisions must be much less than the characteristic dimension (e.g. gap distance) of the system. Moreover, when using the ionization coefficient $\alpha_{\text{eff}}(E/N)$, the local field approximation is used. This requires an efficient relaxation of the electron kinetic energies to the used electron energy distribution function parametrized by the local electric field (the latter being obtained, e.g. from the two-term approximation of the Boltzmann equation). These approximations become inaccurate when there are too few elastic collisions in between ionizing collisions. Using the collision frequency ν_{c} and ionization frequency ν_{i} determined by Bolsig+ as a function of the reduced electric field strength, the limit of the collisional regime can self-consistently be determined to lie within about 500 Td ($\nu_{\text{c}}/\nu_{\text{i}} \approx 100$) and 2000 Td ($\nu_{\text{c}}/\nu_{\text{i}} \approx 10$). A more quantitative analysis of the limits of validity of the drift-diffusion approximation by means of a kinetic electron transport simulation is left to another publication. Incidentally, relating to the question of applicability of the drift-diffusion framework in the local field approximation, one notes that the condition $E/\alpha \gtrsim 20 \cdot U_{\text{i}}$ is not generally valid in typical twisted pair geometries in air, which means that the single avalanche statistics deviates from the exponential distribution observed at low electric field values [31].

Appendix D. On the experimental determination of the reduced coating thickness

If s and ε_{r}' are not known separately already for the considered system (e.g. from data sheets), it is possible to determine the reduced coating thickness $s/\varepsilon_{\text{r}}'$ by a single measurement of the coating's capacitance per unit area C'. From

$$\underline{C}' = \frac{\underline{C}}{A} = \frac{\varepsilon_0 \underline{\varepsilon}_{\text{r}}}{s} \tag{18}$$

it follows that

$$\frac{s}{\underline{\varepsilon}_{\text{r}}} = \frac{\varepsilon_0}{\underline{C}'}. \tag{19}$$

The (complex) reduced coating thickness is thus seen to be inversely proportional to the (complex) capacitance per unit area of the dielectric coating. The latter can be determined by measuring the complex capacitance of the layer through an electrode of known area. The electrode area A can often be determined with better accuracy (e.g. by digital image analysis) than the coating thickness s, which makes this method preferable. In addition, it is interesting to observe that the the influence of the dielectric coating on the PDIV of a wedge-shaped gas gap is determined exclusively by its capacitance per unit area within the quasi-uniform approximation.

Appendix E. Field displacement into gas gap for lossy dielectrics

The voltage drop across the gas gap is influenced by the charge dynamics in the dielectric, which is characterized by the effective complex dielectric permittivity

$$\underline{\varepsilon}_\mathrm{r} = \varepsilon_\mathrm{r}' - j\varepsilon_\mathrm{r}''. \tag{20}$$

The effective permittivity describes the effect of *all* steady state charge motion in the material for a given sinusoidal excitation frequency. The simple voltage transfer relation

$$\frac{U_\mathrm{g}}{U_\mathrm{el}} = \frac{1}{1+\frac{2s}{d\cdot\varepsilon_\mathrm{r}'}} \tag{21}$$

assumes $\varepsilon_\mathrm{r}'' \ll \varepsilon_\mathrm{r}'$ (no phase shift between U_g and U_el), which reduces the validity of equation (21) to low-loss materials. While this condition holds for most relevant insulation materials under 'normal' conditions, the contribution of migrating charge carriers may significantly increase ε_r'' under conditions of, e.g. high temperature and humidity, especially at lower excitation frequencies. The following more general voltage transfer relation must then be used:

$$\frac{U_\mathrm{g}}{U_\mathrm{el}} = \frac{1}{\left|1+\frac{2s}{d\cdot\underline{\varepsilon}_\mathrm{r}}\right|} \overset{!}{=} \frac{1}{1+\frac{2}{d}\left(\frac{s}{\varepsilon_\mathrm{r}'}\right)_\mathrm{eff}}. \tag{22}$$

The voltages here are the magnitudes of the corresponding complex quantities (the phase is not considered here, but could actually be relevant for non-sinusoidal excitations: see appendix F). For a given gap length d, coating thickness s and complex relative permittivity $\underline{\varepsilon}_\mathrm{r}$, the breakdown voltage can still be read out of figure 4, if the ordinate value of $s/\varepsilon_\mathrm{r}'$ is set to the following *effective* value,

$$\left(\frac{s}{\varepsilon_\mathrm{r}'}\right)_\mathrm{eff} \equiv \left|\frac{d}{2}+\frac{s}{\underline{\varepsilon}_\mathrm{r}}\right| - \frac{d}{2}, \tag{23}$$

which follows from equation (22). Note, however, that since $(s/\varepsilon_\mathrm{r}')_\mathrm{eff}$ depends on d, the minimum breakdown voltages for the wedge-shaped configuration must be found not along vertical lines in the $d - s/\varepsilon_\mathrm{r}'$ plane, but the curves defined by equation (23) for a given value of $(s/\varepsilon_\mathrm{r}')_\mathrm{eff}$. Thus, in practice, if only the PDIV is of interest and not its parametrization on a real $s/\varepsilon_\mathrm{r}'$ axis, the more straightforward way is to use equations (7) and (12). This approach is also readily extended to calculate the PDIV under (steady-state) non-sinusoidal voltages (see appendix F).

As expected, when $\tan(\delta) \ll 1$, the approximation $(s/\varepsilon_\mathrm{r}')_\mathrm{eff} \approx s/\varepsilon_\mathrm{r}'$ applies (equation (21)). Physically, the condition $(s/\varepsilon_\mathrm{r}')_\mathrm{eff} \ll s/\varepsilon_\mathrm{r}'$ typically arises in case of charge migration to the blocking gas-dielectric interface, where it builds up a surface charge with a strong screening effect for the interior of the dielectric, yielding a large apparent permittivity in the framework of the simpler analysis (21). Note that the use of a real effective reduced coating thickness in equation (22) disregards the phasor nature of the involved quantities, and is thus only suitable for determining the PDIV of lossy dielectrics under sinusoidal voltages.

Appendix F. Impact of dielectric relaxations on the PDIV under non-sinusoidal voltage excitation

In the main part of this paper, the dielectric response (and the associated modulation of the gap electric field by bound charges) is assumed to be instantaneous. This approximation is good in most cases, but fails if the used permittivity value collects contributions from dipoles with a relaxation time that is longer than the rise time of the electrode voltage. Materials with a larger conductivity are more prone to this effect, as the space charge dipoles associated with the migrating charge carriers typically have relaxation frequencies that coincide with the spectral content of practically relevant voltage waveforms (even the classical 50 Hz sinusoid). In the following, it is shown how to generalize the model to non-sinusoidal periodic voltages, such as the pulse-width-modulated outputs of an inverter.

Consider an arbitrary periodic electrode voltage $U_\mathrm{el}(t)$ of period T. Then a Fourier representation of the type

$$U_\mathrm{el}(t) = \mathrm{Re}\left[\sum_{n=0}^{\infty} \underline{U}_{\mathrm{el},n}\cdot \mathrm{e}^{j\omega_n t}\right] \tag{24}$$

with $\omega_n = n\cdot\frac{2\pi}{T}$ is available. The voltage in the air gap under stationary conditions is then given by

$$U_\mathrm{g}(t) = \mathrm{Re}\left[\sum_{n=0}^{\infty} \frac{\underline{U}_{\mathrm{el},n}}{1+\frac{2s}{d\cdot\underline{\varepsilon}_\mathrm{r}(\omega_n)}}\cdot \mathrm{e}^{j\omega_n t}\right]. \tag{25}$$

When applying an electrode voltage with a large spectral content (e.g. the output of an inverter with large $\mathrm{d}U/\mathrm{d}t$), dielectric relaxations in the excitation bandwidth will produce not only a scaling in the transfer from the electrode to the gap voltage, but also a distortion.

Whether or not the effect is relevant depends on the detailed dielectric response within the signal's bandwidth. The smaller the dispersion of the relative permittivity in the relevant frequency range, the more the voltage transfer approaches the simple scaling

$$U_\mathrm{g}(t) \approx \frac{U_\mathrm{el}(t)}{\left|1+\frac{2s}{d\cdot\underline{\varepsilon}_\mathrm{r}}\right|}. \tag{26}$$

A more detailed analysis of this effect is left to another publication.

Appendix G. Equivalent permittivity of multi-layer dielectric coating

If a N-layer dielectric coating of permittivity values $\{\underline{\varepsilon}_i, i = 1,\ldots,N\}$ and thicknesses $\{s_i, i = 1,\ldots,N\}$ (with $\sum_{i=1}^{N} s_i = s$) is probed by a quasi-uniform electric field, it may be replaced by a homogeneous dielectric of the same total thickness s and an equivalent permittivity of

$$\underline{\varepsilon}_\mathrm{eq} = \left(\sum_{i=1}^{N}\frac{s_i}{s}\cdot\underline{\varepsilon}_i^{-1}\right)^{-1}. \tag{27}$$

This result follows by equating the resulting series capacitance of all layer capacitances $\underline{\varepsilon}_i\cdot A/s_i$ to a single equivalent capacitance $\underline{\varepsilon}_\mathrm{eq}\cdot A/s$. It allows to apply the presented model to multi-layer dielectric coatings, as found in many types of enamelled wires.

Appendix H. A physically motivated parametrization of the effective secondary electron feedback coefficient

As detailed in the follow-up paper investigating the dynamics of the discharge current, the secondary electron feedback coefficient in the presence of both ion and photon feedback can be written as

$$\gamma = \gamma_+ + \gamma_{\mathrm{ph}} \cdot \frac{1}{1 - \frac{\eta_{\mathrm{ph}}}{\alpha_{\mathrm{eff}}}} \cdot \mathrm{e}^{-\eta_{\mathrm{ph}} \cdot d}. \tag{28}$$

The parameter γ_{ph} is simply the average number of secondary photons per ionization event in the gas in the limit of negligible photon absorption, $\eta_{\mathrm{ph}} \to 0$. Note that the photon path has been assumed to follow the electrical field lines in the above derivation, whereas in reality photon path lengths in the gas are on average larger. The model thus works with the lower bound on photon absorption.

When $\alpha_{\mathrm{eff}} \to \eta_{\mathrm{ph}}$, photon feedback is—on average—stifled, because the vast majority of effective photons are absorbed (for $\eta_{\mathrm{ph}} \geqslant \alpha_{\mathrm{eff}}$ the photon contribution to electron feedback is set to zero). The transition from $\alpha_{\mathrm{eff}} > \eta_{\mathrm{ph}}$ to $\alpha_{\mathrm{eff}} < \eta_{\mathrm{ph}}$ takes places at $d \approx 2$ cm in atmospheric pressure air (with the determined value of $\eta_{\mathrm{ph}} = 8\ \mathrm{cm}^{-1}$ and the $\alpha_{\mathrm{eff}}(E)$ parametrization from Hösl *et al* [30] shown in figure 8). A possible and maybe obvious hypothesis could be to assume that the presumably relatively less important secondary feedback by positive ions in small gaps is gradually replacing photon feedback in larger gaps. Alternatively, the relative importance of photo-ionization in the gas bulk (as opposed to the photoelectric effect at the cathode) will gradually increase with increasing gap width, such that the single-avalanche streamer mechanism can be activated. Loeb [57] remarks that for both the Townsend and streamer mechanisms 'we arrive at a general condition for a sparking threshold in terms of the product of two quantities expressing a primary and a secondary process. One secondary process involving *cathode* phenomena leads to a Townsend-type mechanism, the other occurring *in the gas* leads to a streamer mechanism.' (p 160, emphasis in the original). The transition from the Townsend mechanism could then indeed be rather gradual and occur around the gap length where the cathode becomes inefficient as a source of secondary electrons ($\eta_{\mathrm{ph}} = \alpha_{\mathrm{eff}} \to d \approx 2$ cm), such that the secondary feedback in the gas takes over as the dominant source of secondary electrons.

H.1. FE contribution to the secondary electron feedback

It would appear that the FE current density [36]

$$j_{\mathrm{FE}}(E,p) = \mathrm{e} \cdot C \cdot E^2 \cdot \mathrm{e}^{-\frac{D}{E}} \tag{29}$$

($C = 6.7 \cdot 10^3\ \mathrm{ns}^{-1} \cdot \mathrm{kV}^{-2}$, $D = 178\ \mathrm{kV} \cdot \mathrm{mm}^{-1}$) does not fit a description in terms of an electron feedback coefficient, because it simply provides a field-dependent electron current at the cathode. There would then be no unstable mechanism with positive feedback that describes an actual breakdown process. However, as has been shown in [34], the positive ions of the electron avalanches triggered by the field-emitted electrons can enhance the FE yield by their contribution to the cathode field. This process is active only in small gaps, such that the cathode field can reach values of roughly $>20\ \mathrm{kV} \cdot \mathrm{mm}^{-1}$ before breakdown. As shown in [34, 39], ion-enhanced FE can then be incorporated into the Townsend formalism by an additional contribution $\gamma_{\mathrm{FE}} \cdot \mathrm{e}^{-\frac{D}{E}}$ to the effective secondary electron emission coefficient. Combining this result with equation (28) leads to

$$\gamma = \gamma_+ + \gamma_{\mathrm{ph}} \cdot \frac{1}{1 - \frac{\eta_{\mathrm{ph}}}{\alpha_{\mathrm{eff}}}} \cdot \mathrm{e}^{-\eta_{\mathrm{ph}} \cdot d} + \gamma_{\mathrm{FE}} \cdot \mathrm{e}^{-\frac{D}{E}}, \tag{30}$$

where γ_{FE} is a constant. This physically motivated parametrization describes the main features of the measured (deduced) variation of γ with gap distance d (see figure 3). In mid-size atmospheric pressure air gaps (roughly 0.1 mm–1 mm) the secondary feedback is dominated by photon (and possibly ion) feedback, which becomes exponentially less efficient in larger gaps. In microscale gaps ($<100\ \mu$m), the contribution of ion-enhanced FE starts, until it fully dominates the secondary electron supply in gaps of width $<10\ \mu$m.

Although one could as well assume a field-dependent $\gamma_+(E)$ contribution on physical grounds, dropping off in larger gaps to ensure agreement with the measured variation of γ, satisfactory agreement is already obtained with a minimum of free parameters (γ_{ph}, η_{ph} and γ_{FE}) by assuming merely photon feedback to be active in mid-size and larger gaps (i.e. setting $\gamma_+ = 0$). The corresponding values for atmospheric pressure air are $\gamma_{\mathrm{ph}} = 1.5 \cdot 10^{-3}$, $\eta_{\mathrm{ph}} = 8\ \mathrm{cm}^{-1}$ and $\gamma_{\mathrm{FE}} = 0.9$. The corresponding model curve is shown in figure 3 and reported in equation (10).

Appendix I. On the parametrization of the ionization threshold *K*

Let U_{b} be the measured static breakdown voltage of an arbitrary gas gap and $\mathbf{E}(x) = U_{\mathrm{el}} \cdot \mathbf{g}(x)$ the electric field distribution in the gap for an electrode voltage U_{el} (note that although the number of electrons in an avalanche is subject to statistical scatter, the transition of the breakdown probability from $<10^{-9}$ to $>10^{-2}$ occurs in such a small voltage range that it is practically meaningful to speak of *the* static breakdown voltage [12]). Let Π be the collection of all additional physical parameters that affect the static breakdown threshold voltage of the gap, such as gas type and pressure, electrode material and surface roughness, etc. The static breakdown threshold is then—by definition—given by some functional $U_{\mathrm{b}}[\mathbf{g}, \Pi]$.

Assume $\alpha_{\mathrm{eff}}(E)$ to be a non-negative and strongly monotonously increasing function of the electric field strength in the range $E > E_{\mathrm{crit}}$. Its value is assumed to be zero where attachment outweighs ionization and detachment ($E < E_{\mathrm{crit}}$), so that the following integral collects contributions only from within the critical volume (i.e. where $E > E_{\mathrm{crit}}$). If the voltage is large enough to create a non-zero critical volume ($U > U_{\mathrm{crit}}$), then it follows that for any measured breakdown voltage U_{b} there exists a value of $K \in (0, \infty)$ such that

$$\max_{\Gamma\in\Omega}\int_{\Gamma}\alpha_{\mathrm{eff}}(U_{\mathrm{b}}\cdot g(x))\cdot \mathrm{d}x = K, \tag{31}$$

where Ω is the set of field lines in the considered electrode configuration. There is thus always an ionization threshold that correctly predicts the breakdown voltage of a given gaseous insulation gap via the ionization integral criterion. Thus, in order to make a threshold condition on the ionization integral of any use beyond a purely empirical relation, the main challenge is to find a physical parametrization of the function $K[U_{\mathrm{b}},\mathbf{g},\Pi]$. Note that K may itself be a function of U_{b}, as only the effect of the gap voltage on the average avalanche growth is included in the ionization integral.

For example, for quasi-uniform atmospheric pressure air gaps ranging from micrometers to the centimeter gap range ($d \lesssim 2$ cm), the following physical parametrization of the ionization threshold is motivated and validated in this paper:

$$K_{\mathrm{T}}(d) = \ln\left[\frac{\alpha_{\mathrm{eff}}}{\alpha}\cdot\left(\gamma_{\mathrm{ph}}\cdot\frac{1}{1-\frac{\eta_{\mathrm{ph}}}{\alpha_{\mathrm{eff}}}}\cdot \mathrm{e}^{-\eta_{\mathrm{ph}}\cdot d}+\gamma_{\mathrm{FE}}\cdot \mathrm{e}^{-\frac{D}{E}}\right)^{-1}\right], \tag{32}$$

where $E = U/d$ is the macroscopic gap (cathode) electric field, $\gamma_{\mathrm{ph}} = 1.5\cdot 10^{-3}$, $\eta_{\mathrm{ph}} = 8\ \mathrm{mm}^{-1}$, $\gamma_{\mathrm{FE}} = 0.9$ and $D = 178\ \mathrm{kV}\cdot\mathrm{mm}^{-1}$ (see appendix H). In $d \gtrsim 2$ cm gaps, equation (32) must be complemented by a single-avalanche streamer criterion of the Raether–Loeb–Meek type in order to take into account the effect of the single-avalanche space charge on the ionization dynamics (see e.g. [16] and references therein for more details),

$$K_{\mathrm{s}}(d) = \ln\left(\frac{16\pi\varepsilon_0 k}{\xi_{\mathrm{r}}\cdot e}\frac{D_e(E_0)}{\mu_e(E_0)}\cdot d\right) \approx 19 + \ln\left(\frac{d}{1\ \mathrm{cm}}\right). \tag{33}$$

As discussed in appendix H, and shown in equation (9), the physically motivated parametrization of the ionization threshold across the full range of gap distances is then given by $K(d) = \min(K_{\mathrm{T}}(d), K_{\mathrm{s}}(d))$. It should be added that a simple, field-distortion-based streamer inception criterion (33) neglecting the secondary avalanche dynamics in the space-charge-distorted background field represents a rather crude approximation, and may at best be a rough *necessary* condition for streamer inception. Where needed, more sophisticated streamer inception criteria including secondary feedback may be considered (see e.g. [26, 58]).

ORCID iDs

R Färber https://orcid.org/0000-0001-8511-8670
Y Lu https://orcid.org/0000-0002-8909-7827
M Balmelli https://orcid.org/0000-0001-7787-3748
O Sefl https://orcid.org/0000-0003-0868-4614
C M Franck https://orcid.org/0000-0002-2201-7327

References

[1] Hauksbee F 1719 *Physico-Mechanical Experiments on Various Subjects* (J. Senex)
[2] Thomson J J 1906 *Conduction of Electricity Through Gases* (University Press)
[3] Saraiva J, Alemparte C, Belver D, Blanco A, Callón J, Collazo J, Iglesias A and Lopes L 2023 *Nucl. Instrum. Methods Phys. Res.* A **1050** 168183
[4] Balmelli M, Färber R, Merotto L, Soltic P, Bleiner D, Franck C M and Biela J 2021 *IEEE Access* **9** 100050–62
[5] Küchler A 2017 *High Voltage Engineering: Fundamentals-Technology-Applications* (Springer)
[6] IEC 60034–18-41 2014 Rotating electrical machines—part 18–41: partial discharge free electrical insulation systems (type I) used in rotating electrical machines fed from voltage converters—qualification and quality control tests (available at: https://webstore.iec.ch/publication/65356)
[7] Fabiani D, Montanari G C, Cavallini A and Mazzanti G 2004 *IEEE Trans. Dielectr. Electr. Insul.* **11** 393–405
[8] Färber R, Guillod T, Krismer F, Kolar J W and Franck C M 2020 *Energies* **13** 13
[9] Schumann W O 1923 *Elektrische Durchbruchfeldstärke von Gasen* (Springer)
[10] Townsend J 1910 *The Theory of Ionization of Gases by Collision* (Constable Ltd.)
[11] Loeb L B and Meek J M 1940 *J. Appl. Phys.* **11** 438–47
[12] Raether H 1964 *Electron Avalanches and Breakdown in Gases* (Butterworths)
[13] Malik N 1981 *IEEE Trans. Electr. Insul.* **EI-16** 463–7
[14] Chvyreva A, Pancheshnyi S, Christen T and Pemen A 2018 *J. Phys. D: Appl. Phys.* **51** 115202
[15] Verhaart H and Van der Laan P 1984 *J. Appl. Phys.* **55** 3286–92
[16] Färber R and Franck C M 2021 *J. Phys. D: Appl. Phys.* **54** 435202
[17] Lusuardi L, Cavallini A, de la Calle M G, Martínez-Tarifa J and Robles G 2019 *IEEE Electr. Insul. Mag.* **35** 7–15
[18] Pedersen A, McAllister I, Crichton G and Vibholm S 1984 *Arch. Elektrotech.* **67** 395–402
[19] Lusuardi L, Cavallini A, Mancinelli P, De La Calle Manuel G, Martïnez-Tarifa J M and Robles G 2016 Design criteria for inverter-fed type 1 motors *2016 IEEE Int. Conf. on Dielectrics (ICD)* vol 2 pp 605–8
[20] Elorza Azpiazu L, Almandoz G, Egea A, Ugalde G and Badiola X 2023 *Appl. Sci.* **13** 2417
[21] De La Calle M G, Martínez-Tarifa J M, Gómez S A M and Robles G 2020 *IEEE Access* **8** 157510–9
[22] Gutfleisch F and Niemeyer L 1995 *IEEE Trans. Dielectr. Electr. Insul.* **2** 729–43
[23] Meek J M and Craggs J D 1978 *Electrical Breakdown of Gases* (Oxford University Press)
[24] Rogowski W 1936 *Z. Phys.* **100** 1–49
[25] Dhariwal R S, Torres J M and Desmulliez M P Y 2000 *IEE Proc., Sci. Meas. Technol.* **147** 261–5
[26] Nasser E 1971 *Fundamentals of Gaseous Ionization and Plasma Electronics* (*Plasma Physics Series*) (Wiley)
[27] IEC Standard 60851-5 2019 Winding wires—test methods—part 5: electrical properties (available at: https://webstore.iec.ch/publication/65757)
[28] Slade P and Taylor E 2002 *IEEE Trans. Compon. Packag. Manuf. Technol.* **25** 390–6
[29] Go D and Venkattraman A 2014 *J. Phys. D: Appl. Phys.* **47** 503001
[30] Hösl A, Häfliger P and Franck C M 2017 *J. Phys. D: Appl. Phys.* **50** 485207
[31] Legler W 1961 *Z. Naturforsch.* A **16** 253–61
[32] Pancheshnyi S 2013 *J. Phys. D: Appl. Phys.* **46** 155201
[33] Schröder G A 1961 Über den Durchschlag einer Plattenfunkenstrecke in Raumluft bei Elektrodenabständen von 2 bis 9 cm *PhD Thesis* Universität Hamburg
[34] Boyle W and Kisliuk P 1955 *Phys. Rev.* **97** 255
[35] Penney G and Hummert G 1970 *J. Appl. Phys.* **41** 572–7

[36] Balmelli M, Lu Y, Färber R, Merotto L, Soltic P, Bleiner D, Biela J and Franck C M 2022 *IEEE Access* **10** 53454–67
[37] Legler W 1955 *Z. Phys.* **140** 221–40
[38] Meng G, Gao X, Loveless A M, Dong C, Zhang D, Wang K, Zhu B, Cheng Y and Garner A L 2018 *Phys. Plasmas* **25** 082116
[39] Go D B and Pohlman D A 2010 *J. Appl. Phys.* **107** 103303
[40] Warne L K, Jorgenson R E and Nicolaysen S D 2003 Ionization coefficient approach to modeling breakdown in nonuniform geometries *Technical Report* (Sandia National Laboratories (SNL)) (available at: www.osti.gov/biblio/918222)
[41] Gallo C F and Lama W L 1976 *IEEE Trans. Ind. Appl.* **IA-12** 7–11
[42] Lewellyn-Jones F and 1957 *Ionization and Breakdown in Gases* (Methuen)
[43] Ji Y, Giangrande P, Zhao W, Madonna V, Zhang H, Li J and Galea M 2023 *IET Sci. Meas. Technol.* **17** 37–46
[44] Halleck M 1956 *Trans. Am. Inst. Electr. Eng.* III **75** 211–6
[45] Lehr J and Ron P 2017 Foundations of Pulsed Power Technology (Wiley) (available at: https://books.google.ch/books/about/Foundations_of_Pulsed_Power_Technology.html?id=6dgsDwAAQBAJ&redir_esc=y)
[46] Hayakawa N and Okubo H 2005 *IEEE Electr. Insul. Mag.* **21** 5–10
[47] Van de Steen C, Abadie C and Belijar G 2020 Partial discharge detection, experimental-simulation comparison and actual limits *2020 IEEE Electrical Insulation Conf. (EIC)* pp 537–41 (available at: https://ieeexplore.ieee.org/document/9158654)
[48] Calle M G d L, Cleaz Y, Gómez A, Robles G and Martïnez-Tarifa J 2022 Temperature effect on conservative PDIV prediction models based on Paschen's law *2022 IEEE 4th Int. Conf. on Dielectrics (ICD)* pp 336–9 (available at: https://ieeexplore.ieee.org/document/9863528)
[49] Jiang J, Li Z, Li W, Ranjan P, Wei X, Zhang X and Zhang C 2023 *High Volt.* **8** 209–30
[50] Hagelaar G and Pitchford L 2005 *Plasma Sources Sci. Technol.* **14** 722
[51] Lxcat database (available at: https://fr.lxcat.net/) (Accessed 12 December 2020)
[52] Moruzzi J and Price D 1974 *J. Phys. D: Appl. Phys.* **7** 1434
[53] Rao C R and Raju G G 1971 *J. Phys. D: Appl. Phys.* **4** 494
[54] Stout R and Dawson G 1978 *Pure Appl. Geophys.* **116** 159–66
[55] Schumann W O 1923 Über das Minimum der Durchbruchfeldstärke bei Kugelelektroden *Archiv. Für Elektrotechnik* **12** 593–608
[56] Schumann W 1923 *Arch. Elektrotech.* **12** 593–608
[57] Loeb L B 1948 *Rev. Mod. Phys.* **20** 151
[58] Loeb L B and Wijsman R A 1948 *J. Appl. Phys.* **19** 797–9